JOURNAL OF ELECTROMAGNETIC ENGINEERING AND SCIENCE, VOL. 25, NO. 1, 85~91, JAN. 2025

https://doi.org/10.26866/jees.2025.1.r.281
ISSN 2671-7263 (Online) · ISSN 2671-7255 (Print)

Enhancing 2-D Beam Scanning Capability through Extended Transmission Paths in a Liquid Crystal-Based Transmitarray Antenna for mmWave Communications

Seungwoo Bang · Hogyeom Kim · Jungsuek Oh*

Abstract

This paper introduces a novel method for implementing a liquid crystal-based transmitarray (LCTA) antenna with two-dimensional (2D) beam scanning capability for the first time. Extending the phase tuning range of LCTA unit cells faces a crucial limitation in maintaining a thin single liquid crystal (LC) layer because the tuning range is significantly dependent on the LC thickness. The proposed transmission line-based unit cell design could overcome this limitation due to its horizontal propagation characteristic among the LC layers. Therefore, the proposed LCTA unit cell achieves a phase tuning range of 130° while maintaining the thickness of the LC under 0.25 mm at 28 GHz. Furthermore, a 10 × 10 array design is fabricated and measured to verify its 2D beam scanning capability. Consequently, the maximum scanning angle of 30° is obtained in the E-plane and H-plane from measurements. Comparative results with previous studies also emphasize the advantages of the proposed design.

Key Words: Liquid Crystal, Metasurface, mmWave Communication, Transmitarray.

I. Introduction

Metasurfaces such as transmitarrays (TAs), reflectarrays (RAs), and Metasurface-empowered antennas, are attractive structures that can achieve high gain, wide bandwidth, and beam-reconfigurable performance, possessing planar, lightweight, and easily fabricated properties [1–8]. TAs, in particular, have received significant attention due to their ability to refract the radiation beam on the desired direction by compensating for the phase of the incident electromagnetic (EM) wave. Therefore, TAs play a decisive role in high-frequency applications such as mmWave base stations, automotive radar systems, and satellite communications [8–10].

In general, there are two types of TAs: passive and active. The former steers the main beam with phase shifters or switching circuits connected to the source antenna [11, 12]. However, this type of TA requires the integration of additional components on the radio-frequency (RF) integrated circuit. The interconnections between these components increase the complexity of the circuits and RF power consumption, leading to excessive insertion loss [13].

In contrast, the latter type metamorphoses its EM properties, that is, phase responses, in the spatial domain. This characteristic can overcome the disadvantages of a passive TA. Fig. 1 illustrates the operational principle of a liquid crystal-based transmitarray (LCTA), which belongs to the category of active TAs. Liquid

Manuscript received March 01, 2024 ; Revised May 23, 2024 ; Accepted June 11, 2024. (ID No. 20240301-044J)
Institute of New Media and Communications, Electrical and Computer Engineering, Seoul National University, Seoul, Korea.
*Corresponding Author: Jungsuek Oh (e-mail: jungsuek@snu.ac.kr)

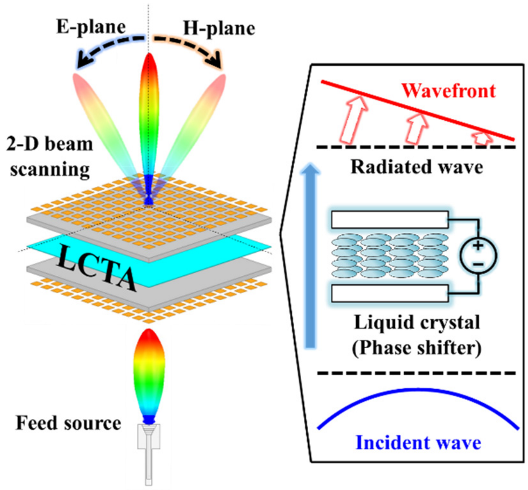

Fig. 1. Operation principle of an LCTA. The LCTA compensates for a phase of an incident wavefront from the feed source.

crystal (LC) adjusts the phase of the wavefront after the TA receives an RF signal from the feed antenna. Consequently, the direction of the EM wave radiated from the TA can be reconfigured.

Recently, active TAs have been investigated by employing active components or metamaterials such as PIN diodes, varactors, and LCs [14–18]. While PIN diodes have an advantage in beam-steering performance, the undesirable power consumption resulting from changing the on/off states by controlling currents can decrease the efficiency of systems. On the other hand, varactors vary the capacitance by applying voltages without currents flowing through the bias circuit. Varactors also provide a continuous change in the phase response, while PIN diodes result in discrete responses. However, these types of active components need to be mounted on substrates, making them vulnerable to external collisions. Furthermore, active components have limited operating frequencies due to their self-resonance frequencies. Unlike active components, an LC transforms its permittivity with various DC bias voltages. Additionally, an LC has the advantage of operating at high frequencies since it lacks a self-resonance frequency. Furthermore, mass-produced LCs cost little.

For the reasons mentioned above, LC-based metasurfaces are currently under active study [16–23]. However, while RAs and active frequency selective surfaces with LC have been widely investigated in recent decades, the LCTA-related research field remains limited. Due to the narrow tuning range of the permittivity in LC, the beam coverage of LCTA faces a crucial limitation when it is implemented in real-world communication systems. In [18], for instance, only achieved the maximum scan angle of $\pm 5°$.

This is the first study to propose an LCTA focusing on the mmWave communication band with a two-dimensional (2D) beam scanning capability. To achieve a wide tunable phase shift range despite the limited variance of permittivity, the meander line embedded in a substrate-integrated waveguide (SIW) unit cell structure is implemented. The unit cell consists of receive–transmit antennas and transmission lines such as SIW and stripline, where the unit cell receives the RF signal from the feeding source and transmits it to the far field with phase compensation. Typically, the incident EM wave propagates conventional unit cells vertically (i.e., through LC thickness). In contrast, in the proposed unit cell, the EM wave travels along the transmission lines horizontally due to the antenna–SIW transitions in the unit cell (Fig. 2). Due to the horizontal propagation of the EM wave in the unit cell, the electrical length of the unit cell increases drastically more than in traditional unit cell structures.

In Section II, the design of the proposed LCTA unit cell is introduced with the simulated frequency responses. Section III rovides the measurement setup and results of radiation patterns. Finally, Section IV concludes the study.

II. LCTA DESIGN PRINCIPLES

1. Phase Tuning Range Expansion

In microwave theory, the phase delay φ of the transmission line is defined as:

$$\varphi = \beta \ell, \tag{1}$$

$$\beta = \omega\sqrt{\mu\varepsilon}, \tag{2}$$

where ω is the angular frequency (i.e., $\omega = 2\pi f$), ℓ is the physical length of the transmission line, and μ and ε are the permeability and permittivity of the material filled in the transmission line, respectively [23]. To induce a phase variation in the two-port system at the same frequency, either the physical length or material property must be changed (i.e., $\Delta\varphi = \beta\Delta\ell$ or $\Delta\varphi = \Delta\beta\ell$).

Hence, the LC-based unit cells vary their phase tuning range by changing their material properties. However, LC-based unit cells typically have a narrow phase tuning range due to the limited range of the dielectric constant. The tunable range of the dielectric constant of the LC used in this paper increases from 2.5 to 3.5 (Merck GT7-29001) where the loss tangent decreases from 0.012 to 0.0064 [21, 22]. In this case, the simplest way to expand the tuning range is by increasing the length of the wave propagation (Fig. 2(a)). Thus, Maasch et al. [18] proposed a fishnet structure with two thick layers of LC substrates. From (1) and (2), we can assume that using two layers of thick LC substrates can significantly increase the phase tuning range. Although this methodology can expand the tuning range, the fabrication process would be complicated because of the increased bias circuits and increased cost compared to using a thin single LC layer. Therefore, this paper proposes the meander line structure on the LC substrate to increase the tunable range without using an additional LC layer. Unlike the conventional structure, the incident wave

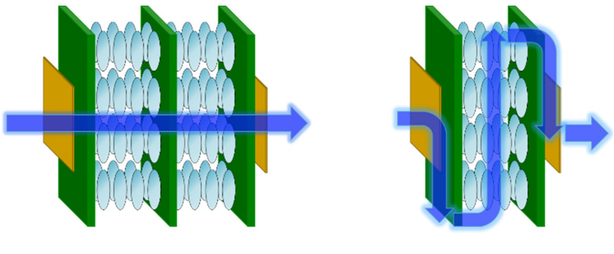

(a) (b)

Fig. 2. Examples of ways to expand the phase tuning range: (a) increasing LC thickness (conventional) and (b) converting transmission path (proposed).

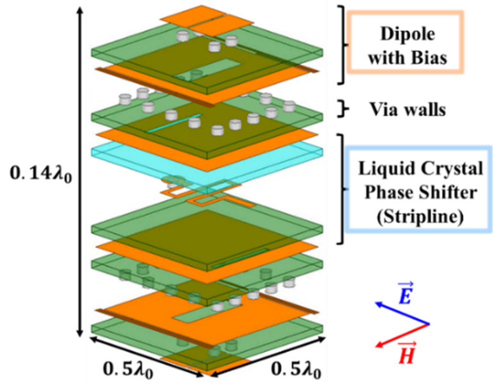

Fig. 3. Exploded view of the proposed unit cell design.

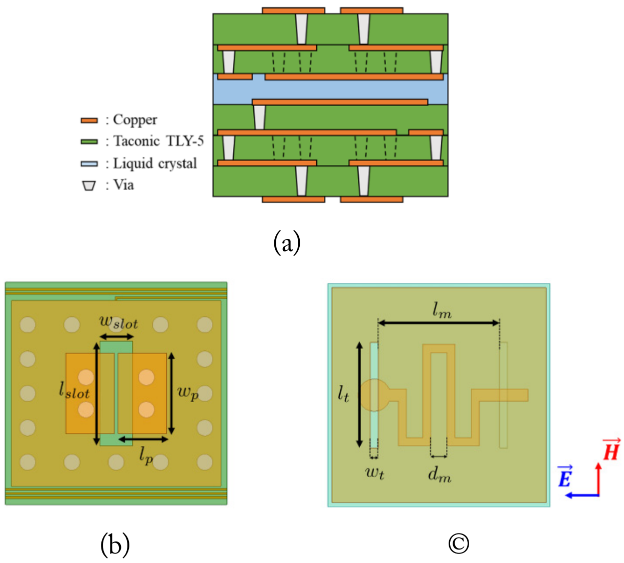

Fig. 4. Geometry of the unit cell: (a) unit cell cross-section on E-plane (black dash: via wall), (b) dipole layer, and (c) stripline layer; w_p=1.8, l_p=1.4, w_{slot}=0.9, l_{slot}=2.6, w_t=0.2, l_t=2.6, d_m=0.4, and l_m=3.0 (unit: mm).

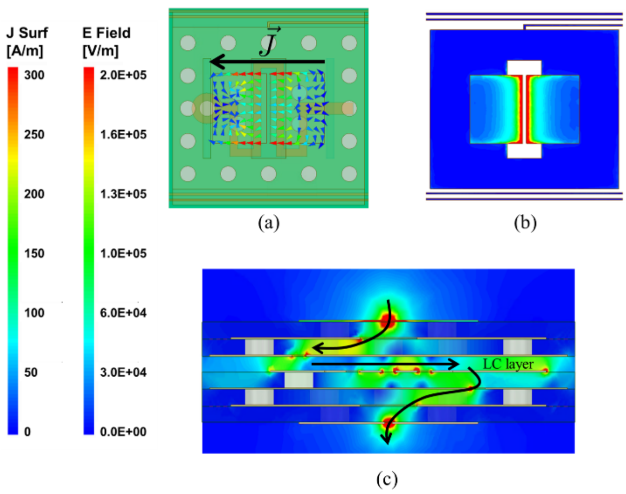

Fig. 5. Field distribution of the proposed unit cell design: (a) top view (current vector), (b) top view (E-field on dipole and bias layer), and (c) unit cell cross-section on E-plane (E-field).

propagates horizontally on the LC layer, extending the length of the transmission line from the thickness to the width of the substrate. Fig. 2(b) illustrates the proposed unit cell design concept.

2. Unit Cell Design

Figs. 3 and 4 show the exploded view and detailed geometry of the proposed unit cell design. After the antenna receives the EM wave from the feed source, shorting vias among the patch and slotted ground can guide the wave to the SIW structure [25]. The SIW structure prevents leakage of the EM wave that interferes with the adjacent unit cells and bias lines. To guide the wave along the meander line, the transition between a slot and a stripline is employed.

On the top and bottom layers, magnetoelectric dipole antennas are adopted to facilitate the guidance of the incident wave from the antenna to the SIW structure. Fig. 5(a) plots the surface current vector of the magnetoelectric dipole on the unit cell to clarify the polarization characteristic. The polarization of the dipole layer maintains its direction despite the transmission lines being embedded in the LC substrate. As shown in Fig. 5(b), the electric field is concentrated strongly on the gap between the patches. This field excites the TE_{10} mode of the SIW and guides the wave to the next layers. To utilize the meander line for a wider phase tuning range, the SIW and meander stripline are coupled through the slot transition. Fig. 5(c) shows the electric field among the unit cell cross-section on the E-plane. The notable aspect is the propagation path inside the LC layer, which propagates horizontally guided by the meander line structure.

Fig. 6 shows the simulated S_{21} responses with respect to the relative permittivity of the LC. The proposed unit cell design achieves a phase tuning range of 130° while maintaining the insertion loss level under 6 dB for the frequency point of 28 GHz. Fig. 7 depicts frequency responses affected by the number of bias lines. The number inside the bracket of the legend refers to the relative permittivity of the LC layer. The frequency responses of the unit cell regarding the number of bias lines are unchanged because the via walls block the E-field excitation on the bias lines (Fig. 5(b)).

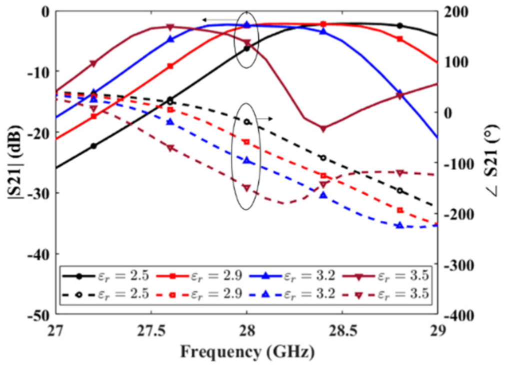

Fig. 6. Frequency responses of the unit cell regarding the LC permittivity.

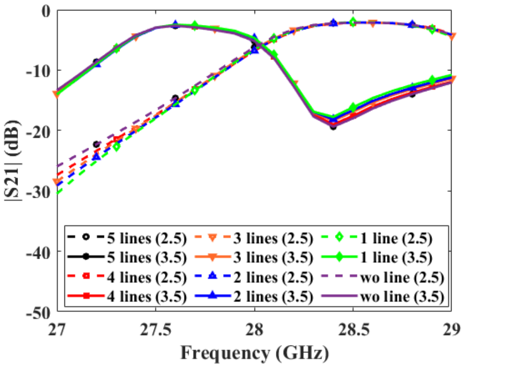

Fig. 7. Frequency responses of the unit cell regarding the number of bias lines. Numbers inside the brackets refer to the LC permittivity.

III. FABRICATION AND MEASUREMENT RESULT

A fabricated example of the proposed LCTA sample is shown in Fig. 8. The radiating region of the LCTA is 52 mm × 52 mm, and the supplemental area consists of DC bias connections. The Taconic TLY-5 substrate (ε_r = 2.2 and tanδ = 0.0009) is used with a thickness of 0.25 mm for all substrate layers. Fig. 9 depicts the measurement setup of the proposed LCTA. The distance between the receiver horn and LCTA is 1.5 m, which satisfies the far field condition (i.e., distance $> 2D^2/\lambda_0$ at 28 GHz where D = $\sqrt{2} \times 52$ mm). The DC bias control unit is connected to the LCTA and the laptop. This bias unit can apply voltage levels from 0 to 20 V for 100 channels. Therefore, the number of unit cells in the LCTA is also 100 (i.e., a 10 × 10 array) due to the control unit channel allowance. To match the bias voltage level and the relative permittivity of the LC layer, the vector network analyzer (VNA) MS4647A from Anritsu is connected to the TRx pair, and the control unit applies the same voltage to all the unit cells. Fig. 10 shows the phase difference with respect to the LC permittivity and DC bias voltage, representing simulation and measurement results, respectively. There is a discrepancy in operating frequency between the simulated and measured results because the PCB was fabricated in-house, which led to inaccurate etching processes, misaligned layers, LC leakage through vias, and unexpected minor errors.

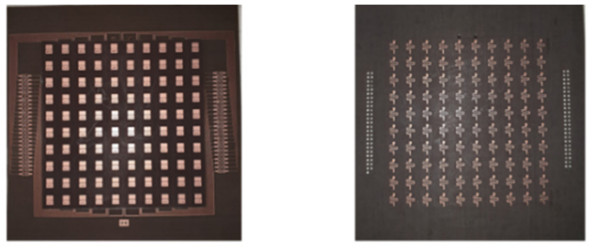

(a) (b)

Fig. 8. A photograph of the fabricated sample: (a) dipole layer with bias lines, and (b) meander layer.

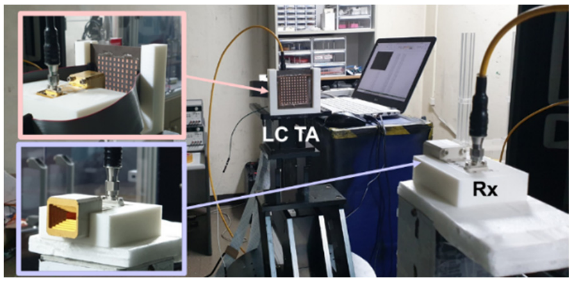

Fig. 9. Measurement setup.

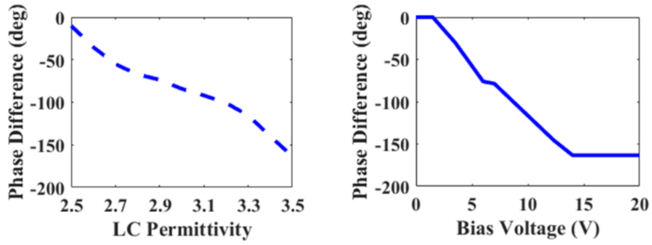

(a) (b)

Fig. 10. Simulated and measured results of phase differences of the LCTA unit cell (Sim: at 28 GHz, Meas: at 28.5 GHz).

In Fig. 11, the simulated and measured radiation patterns of the proposed design are shown. From this figure, it is evident that the proposed LCTA can steer the main beam direction to 30° not only in the E-plane but also in the H-plane. The 2D beamforming capability was achieved because its SIW structure isolates the DC connections between adjacent unit cells. The peak gains of the simulated and measured results are 14.5 and 6.1 dBi, respectively.

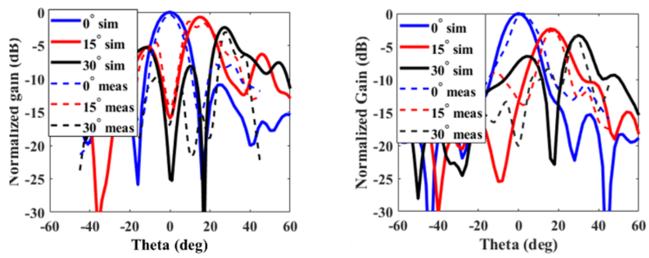

(a) (b)

Fig. 11. Simulated and measured radiation pattern results on (a) E-plane and (b) H-plane (Sim: at 28 GHz, Meas: at 28.5 GHz).

Table 1. Comparison with previous studies

	Freq. (GHz)	LC thickness (mm)	Number of LC layers	Phase tuning range (°)	FoM (°/mm)	Beam scanning capability	Max. steering angle (°)
Foo [16][a]	39	0.1	8	360	450	2D	20
Li et al. [17][a]	340	0.58	2	180	155	1D	40
Maasch et al. [18]	27.5	0.762	2	180	118	1D	5
This work	28	0.25	1	130	520	2D	30

[a]Simulated results only.

Table 1 shows the comparative results of previous studies on LCTA [16–18]. A comparison of operating frequency, LC thickness, number of LC layers, phase tuning range, beam scanning capability, and maximum steering angle is conducted. The figure of merit (FoM) is defined as the ratio of the maximum phase tuning range over the LC thickness:

$$FoM = \frac{\Delta\varphi}{Total\ LC\ thickness\ (\mathrm{mm})}. \tag{3}$$

The remarkable feature of the proposed LCTA is the 2D beam scanning capability with the thin single LC layer.

IV. Conclusion

In this paper, an LCTA antenna achieving 2D beam scanning capability for mmWave communication is implemented. It is observed that manipulating the propagation path among the unit cell horizontally could extend the phase tuning range of the thin LC layer-based unit cell design. The narrow scanning range of conventional LCTAs is overcome by adopting the proposed method, steering the main beam to 30°. Despite the persistent practical limitations of LCTA, this paper presents for the first time the feasibility of a 2D beam-steering LCTA that has been both fabricated and measured. Additionally, the proposed LCTA unit cell employs a concept that broadens the phase tuning range while using a minimal amount of LC layer.

This work was supported by Samsung Research Funding Center of Samsung Electronics (Project No. SRFC-TE2103).

References

[1] A. H. Abdelrahman, F. Yang, A. Z. Elsherbeni, P. Nayeri, and C. A. Balanis, *Analysis and Design of Transmitarray Antennas.* Cham, Switzerland: Springer, 2017. https://doi.org/10.1007/978-3-031-01541-0

[2] D. Seo, H. Kim, S. Oh, J. Kim, and J. Oh, "Ultrathin high-gain D-band transmitarray based on a spatial filter topology utilizing bonding layer effect," *IEEE Antennas and Wireless Propagation Letters*, vol. 21, no. 10, pp. 1945-1949, 2022. https://doi.org/10.1109/LAWP.2022.3186686

[3] E. Zhou, Y. Cheng, F. Chen, and H. Luo, "Wideband and high-gain patch antenna with reflective focusing metasurface," *AEU-International Journal of Electronics and Communications*, vol. 134, article no. 153709, 2021. https://doi.org/10.1016/j.aeue.2021.153709

[4] E. Zhou, Y. Cheng, F. Chen, H. Luo, and X. Li, "Low-profile high-gain wideband multi-resonance microstrip-fed slot antenna with anisotropic metasurface," *Progress In Electromagnetics Research*, vol. 175, pp. 91-104, 2022. https://doi.org/10.2528/PIER22062201

[5] J. Wang, J. Zhao, Y. Cheng, H. Luo, and F. Chen, "Dual-band high-gain microstrip antenna with a reflective focusing metasurface for linear and circular polarizations," *AEU-International Journal of Electronics and Communications*, vol. 157, article no. 154413, 2022. https://doi.org/10.1016/j.aeue.2022.154413

[6] Z. Zhang, Y. Cheng, H. Luo, and F. Chen, "Low-profile wideband circular polarization metasurface antenna with characteristic mode analysis and mode suppression," *IEEE Antennas and Wireless Propagation Letters*, vol. 22, no. 4, pp. 898-902, 2023. https://doi.org/10.1109/LAWP.2022.3227881

[7] B. Kim, J. Jung, S. Yun, H. Kim, and J. Oh, "Heterogeneous metasurface empowering proximate high-permittivity ceramic cover for a 5G dual-band millimeter-wave smartphone," *IEEE Transactions on Antennas and Propagation*, vol. 72, no. 5, pp. 4086-4094, 2024. https://doi.org/10.1109/TAP.2024.3383725

[8] Y. Kim, H. Kim, I. Yoon, and J. Oh, "4×8 patch array-fed FR4-based transmit array antennas for affordable and reliable 5G beam steering," *IEEE Access*, vol. 7, pp. 88881-88893, 2019. https://doi.org/10.1109/ACCESS.2019.2926379

[9] S. B. Yeap, X. Qing, and Z. N. Chen, "77-GHz dual-layer transmit-array for automotive radar applications," *IEEE Transactions on Antennas and Propagation*, vol. 63, no. 6, pp. 2833-2837, 2015. https://doi.org/10.1109/TAP.2015.2419691

[10] H. Hasani, J. S. Silva, S. Capdevila, M. Garcia-Vigueras, and J. R. Mosig, "Dual-band circularly polarized transmitarray antenna for satellite communications at (20, 30) GHz," *IEEE Transactions on Antennas and Propagation*, vol. 67, no. 8, pp. 5325-5333, 2019. https://doi.org/10.1109/TAP.2019.2912495

[11] E. Shin and J. Oh, "Beam-steerable passive transmitarray optimized based on an adjacent algorithm," *IEEE Access*, vol. 9, pp. 28797-28804, 2021. https://doi.org/10.1109/ACCESS.2021.3058647
[12] J. G. Lee, T. S. Kwon, and J. H. Lee, "Beam pattern reconfigurable circularly polarized transmitarray antenna by rearrangement of sources," *Microwave and Optical Technology Letters*, vol. 61, no. 4, pp. 999-1003, 2019. https://doi.org/10.1002/mop.31657
[13] J. Oh, "Millimeter-wave thin lens employing mixed-order elliptic filter arrays," *IEEE Transactions on Antennas and Propagation*, vol. 64, no. 7, pp. 3222-3227, 2016. https://doi.org/10.1109/TAP.2016.2559582
[14] J. Kim, J. Kim, J. H. Oh, S. H. Wi, and J. Oh, "Rotated feed-combined reconfigurable transmit RIS with disparate deployment of 1-bit hybrid units for B5G/6G," *IEEE Transactions on Antennas and Propagation*, vol. 71, no. 6, pp. 5457-5462, 2023. https://doi.org/10.1109/TAP.2023.3248374
[15] M. Frank, F. Lurz, R. Weigel, and A. Koelpin, "Electronically reconfigurable 6×6 element transmitarray at K-band based on unit cells with continuous phase range," *IEEE Antennas and Wireless Propagation Letters*, vol. 18, no. 4, pp. 796-800, 2019. https://doi.org/10.1109/LAWP.2019.2903338
[16] S. Foo, "Liquid-crystal reconfigurable, lens-enhanced, millimeter-wave phased array," in *Proceedings of the 12th European Conference on Antennas and Propagation (EuCAP)*, London, UK, 2018, pp. 1-5. https://doi.org/10.1049/cp.2018.0677
[17] X. Li, Z. Li, C. Wan, and S. Song, "Design and analysis of terahertz transmitarray using 1-bit liquid crystal phase shifter," in *Proceedings of 2020 9th Asia-Pacific Conference on Antennas and Propagation (APCAP)*, Xiamen, China, 2020, pp. 1-2. https://doi.org/10.1109/APCAP50217.2020.9246116
[18] M. Maasch, M. Roig, C. Damm, and R. Jakoby, "Voltage-tunable artificial gradient-index lens based on a liquid crystal loaded fishnet metamaterial," *IEEE Antennas and Wireless Propagation Letters*, vol. 13, pp. 1581-1584, 2014. https://doi.org/10.1109/LAWP.2014.2345841
[19] H. Kim, J. Kim, and J. Oh, "Communication a novel systematic design of high-aperture-efficiency 2D beam-scanning liquid-crystal embedded reflectarray antenna for 6G FR3 and radar applications," *IEEE Transactions on Antennas and Propagation*, vol. 70, no. 11, pp. 11194-11198, 2022. https://doi.org/10.1109/TAP.2022.3209178
[20] Y. Youn, D. An, D. Kim, M. Hwang, H. Choi, B. Kang, and W. Hong, "Liquid crystal-driven reconfigurable intelligent surface with cognitive sensors for self-sustainable operation," *IEEE Transactions on Antennas and Propagation*, vol. 71, no. 12, pp. 9415-9423, 2023. https://doi.org/10.1109/TAP.2023.3312814
[21] H. Kim, S. Oh, S. Bang, H. Yang, B. Kim, and J. Oh, "Independently polarization manipulable liquid-crystal-based reflective metasurface for 5g reflectarray and reconfigurable intelligent surface," *IEEE Transactions on Antennas and Propagation*, vol. 71, no. 8, pp. 6606-6616, 2023. https://doi.org/10.1109/TAP.2023.3283136
[22] H. Yang, S. Kim, H. Kim, S. Bang, Y. Kim, S. Kim, K. Park, D. Kwon, and J. Oh, "Beyond limitations of 5G with RIS: Field trial in a commercial network, recent advances, and future directions," *IEEE Communications Magazine*, vol. 64, no. 10, pp. 132-138, 2024. https://doi.org/10.1109/MCOM.024.2300440
[23] B. Moon, S. Bang, H. Kim, and J. Oh, "Simultaneously dual-polarization convertible sub-THz reconfigurable intelligent surface enabled by through-quartz VIAs," in *Proceedings of 2024 18th European Conference on Antennas and Propagation (EuCAP)*, Glasgow, UK, 2024, pp. 1-5. https://doi.org/10.23919/EuCAP60739.2024.10501659
[24] D. M. Pozar, *Microwave Engineering*, 4th ed. Hoboken, NJ: John Wiley & Sons, 2011.
[25] Z. W. Miao, Z. C. Hao, G. Q. Luo, L. Gao, J. Wang, X. Wang, and W. Hong, "140 GHz high-gain LTCC-integrated transmit-array antenna using a wideband SIW aperture-coupling phase delay structure," *IEEE Transactions on Antennas and Propagation*, vol. 66, no. 1, pp. 182-190, 2018. https://doi.org/10.1109/TAP.2017.2776345

Seungwoo Bang
https://orcid.org/0000-0003-4341-3270

received a B.S. degree from Seoul National University of Science and Technology, South Korea, in 2022. He is currently pursuing an integrated master's and Ph.D. at the Department of Electrical and Computer Engineering at Seoul National University, South Korea. His current research interests include metasurface and antenna design.

Hogyeom Kim
https://orcid.org/0000-0001-7196-2002

received a B.S. degree in electrical engineering from Inha University, Korea, in 2016. He served in the Korea Army from 2016 to 2018. Currently, he is pursuing a Ph.D. degree at Seoul National University, Korea. His current research interests include transmit/reflectarray antennas, reconfigurable intelligence surfaces for B5G/6G communication, and millimeter-wave radar systems. Also, liquid-crystal material-based metasurface is one of his research topics.

Jungsuek Oh
https://orcid.org/0000-0002-2156-4927

received his B.S. and M.S. degrees from Seoul National University, Korea, in 2002 and 2007, respectively, and a Ph.D. degree from the University of Michigan at Ann Arbor in 2012. From 2007 to 2008, he was with Korea Telecom as a hardware research engineer, working on the development of flexible RF devices. In 2012, he was a postdoctoral research fellow in the Radiation Laboratory at the University of Michigan. From 2013 to 2014, he was a staff RF engineer with Samsung Research America, Dallas, working as a project leader for the 5G/millimeter-wave antenna system. From 2015 to 2018, he was a faculty member in the Department of Electronic Engineering at Inha University in South Korea. He is currently an Associate Professor in the School of Electrical and Computer Engineering, Seoul National University, South Korea. His research areas include mmWave beam focusing/shaping techniques, antenna miniaturization for integrated systems, and radio propagation modeling for indoor scenarios. He is the recipient of the 2011 Rackham Predoctoral Fellowship Award at the University of Michigan. He has published more than 50 technical journal and conference papers, and has served as a technical reviewer for the *IEEE Transactions on Antennas and Propagation*, *IEEE Antenna and Wireless Propagation Letters*, and so on. He has served as a TPC member and as a session chair for the IEEE AP-S/USNC-URSI and ISAP. He has been a senior member of IEEE since 2017.